Proceedings of the Korean Nuclear Society Spring Meeting
Kori, Korea, May 2000

Development of the Two-Dimensional Hot Pool Model for Pool-Type Liquid Metal Reactors

Yong-Bum Lee, Seok-Ki Choi, Young Min Kwon, Won Pyo Chang and Dohee Hahn

Korea Atomic Energy Research Institute
KALIMER Technology Development Team
Yusong P.O. Box 105, Taejon, Korea 305-600

Abstract

The SSC-K code is developed at KAERI on the basis of SSC-L originally developed at BNL to analyze loop-type LMR transient. Because the dynamic response of the primary coolant in a pool-type LMR, particularly the hot pool concept, can be quite different from that in the loop-type LMR, the major modifications of SSC-L have been made for the safety analysis of KALIMER. In particular, it is necessary to predict the hot pool coolant temperature distribution with sufficient accuracy to determine the inlet temperature conditions for the IHXs because the temperature distribution of hot pool can alter the overall system response. In this paper two-dimensional hot pool model is developed and is applied to the SSC-K code. A preliminary evaluation of some unprotected accidents for the KALIMER design with updated SSC-K code has been performed and analyzed.

1. Introduction

The Super System Code of KAERI (SSC-K) is developed at Korea Atomic Energy Research Institute (KAERI) on the basis of SSC-L originally developed at BNL to analyze loop-type LMR (Liquid Metal Reactor) transient [1]. Because the dynamic response of the primary coolant in a pool-type LMR, particularly the hot pool concept, can be quite different from that in the loop-type LMR, the major modifications of SSC-L have been made for the safety analysis of KALIMER [2]. The major difference between KALIMER and general loop-type LMRs exists in the primary heat transport system. In KALIMER, all of the essential components composing the primary heat transport system are located within the reactor vessel. They include the reactor, four EM pumps, the primary side of four intermediate heat exchangers, sodium pools, cover gas blanket, and associated pipings. This is contrast to the loop-type LMRs, in which all the primary components are connected via piping to form loops external to the reactor vessel.

During a normal reactor scram, the heat generation is reduced almost instantaneously while the coolant flow rate follows the pump coastdown. This

mismatch between power and flow results in a situation where the core flow entering the hot pool is at a lower temperature than the temperature of the bulk pool sodium. This temperature difference leads to thermal stratification. Thermal stratification can occur in the hot pool region if the entering coolant is colder than the existing hot pool coolant and the flow momentum is not large enough to overcome the negative buoyancy force. Since the fluid of hot pool enters IHXs, the temperature distribution of hot pool can alter the overall system response. Hence, it is necessary to predict the pool coolant temperature distribution with sufficient accuracy to determine the inlet temperature conditions for the IHXs and its contribution to the net buoyancy head.

Therefore, in this paper two-dimensional hot pool model is developed instead of existing one-dimensional model to predict the hot pool coolant temperature and velocity distribution more accurately and is applied to the SSC-K code. A preliminary evaluation of some unprotected accidents for the KALIMER design has been performed with existing one-dimensional and developed two-dimensional hot pool model. Also the comparisons between one-dimensional and two-dimensional hot pool model are performed and analyzed.

2. General Modeling Description

Figure 1 shows a schematic diagram of SSC-K modeling for KALIMER. KALIMER has only one cover gas space and the IHX outlet is directly connected to cold pool. Since the sodium in the hot pool is separated from the cold pool by insulated barrier in KALIMER, the liquid level in the hot pool is different from that in the cold pool mainly due to hydraulic losses and pump suction heads occurring during flow through the circulation paths. In some accident conditions the liquid in the hot pool is flooded into cold pool and forms a natural circulation flow path. During the loss of heat sink transients, this will provide as a major heat removal mechanism with the passive decay heat removal system. Since the pipes in the primary system exists only between the pump discharge and the core inlet plenum and are submerged in the cold pool, a pipe rupture accident becomes less severe because of a constant back pressure exerted against the coolant flow from break.

2.1 One-Dimensional Hot Pool Model

The core flow in the hot pool is represented by a two-zone model. The hot pool is divided into two perfectly mixing zones determined by the maximum penetration distance of the core flow. This penetration distance is a function of the Froude number of the average core exit flow. The temperature of each zone is computed from energy balance considerations. The temperature of the upper portion, T_A, will be relatively unchanged; in the lower region, however, T_B will be changed

and somewhat between the core exit temperature and the temperature of the upper zone due to active mixing with core exit flow as well as heat transfer with the upper zone. The temperature of upper zone is mainly affected by interfacial heat transfer.

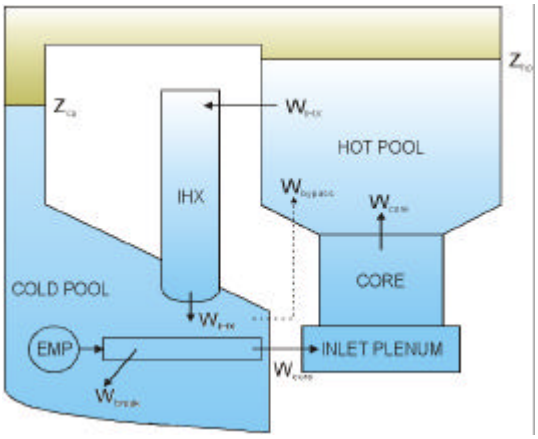

Fig. 1 Schematic of SSC-K modeling for KALIMER

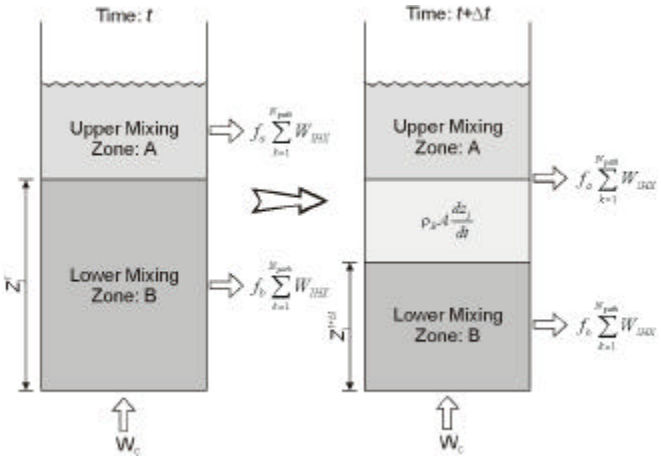

Fig. 2 One-dimensional two-mixing zone model

2.2 Two-Dimensional Hot Pool Model

2.2.1 Governing Equations

The governing equations for conservation of mass, momentum, energy, turbulent kinetic energy and rate of turbulent kinetic energy dissipation for k-ε turbulence model in a generalized coordinate system x^j can be written as follows;

$$\frac{\partial}{\partial x^1}(rU_1) + \frac{\partial}{\partial x^2}(rU_2) = 0 \tag{1}$$

$$\frac{\partial}{\partial t}(rJ\rho u_1) + \frac{\partial}{\partial x^1}\left[rU_1u_1 - \frac{r}{J}(\mu+\mu_t)\left\{\frac{\partial u_1}{\partial x^1}B_1^1 + \frac{\partial u_1}{\partial x^2}B_2^1 + b_1^1w_1^1 + b_2^1w_1^2\right\} + rb_1^1p\right]$$
$$+\frac{\partial}{\partial x^2}\left[rU_2u_1 - \frac{r}{J}(\mu+\mu_t)\left\{\frac{\partial u_1}{\partial x^1}B_1^2 + \frac{\partial u_1}{\partial x^2}B_2^2 + b_1^2w_1^1 + b_2^2w_1^2\right\} + rb_1^2p\right] = 0. \tag{2}$$

$$\frac{\partial}{\partial t}(rJ\rho u_2)\frac{\partial}{\partial t}(rJ\rho u_1)$$
$$+\frac{\partial}{\partial x^1}\left[rU_1u_1 - \frac{r}{J}(\mu+\mu_t)\left\{\frac{\partial u_1}{\partial x^1}B_1^1 + \frac{\partial u_1}{\partial x^2}B_2^1 + b_1^1w_1^1 + b_2^1w_1^2\right\} + rb_1^1p\right]$$
$$+\frac{\partial}{\partial x^2}\left[rU_2u_1 - \frac{r}{J}(\mu+\mu_t)\left\{\frac{\partial u_1}{\partial x^1}B_1^2 + \frac{\partial u_1}{\partial x^2}B_2^2 + b_1^2w_1^1 + b_2^2w_1^2\right\} + rb_1^2p\right] = 0. \tag{3}$$

$$\frac{\partial}{\partial t}(rJ\rho T)+\frac{\partial}{\partial x^1}\left[rU_1T-\frac{r}{J}(\frac{\mu}{P_r}+\frac{\mu_t}{P_{\eta}})\left\{\frac{\partial T}{\partial x^1}B_1^1+\frac{\partial T}{\partial x^2}B_2^1\right\}\right]$$
$$+\frac{\partial}{\partial x^2}\left[rU_2T-\frac{r}{J}(\frac{\mu}{P_r}+\frac{\mu_t}{P_{\eta}})\left\{\frac{\partial T}{\partial x^1}B_1^2+\frac{\partial T}{\partial x^2}B_2^2\right\}\right]=0. \tag{4}$$

$$\frac{\partial}{\partial t}(rJ\rho k)+\frac{\partial}{\partial x^1}\left[rU_1k-\frac{r}{J}(\mu+\frac{\mu_t}{\sigma_k})\left\{\frac{\partial k}{\partial x^1}B_1^1+\frac{\partial k}{\partial x^2}B_2^1\right\}\right]$$
$$+\frac{\partial}{\partial x^2}\left[rU_2k-\frac{r}{J}(\mu+\frac{\mu_t}{\sigma_k})\left\{\frac{\partial k}{\partial x^1}B_1^2+\frac{\partial k}{\partial x^2}B_2^2\right\}\right]=rJ(G-\rho\varepsilon) \tag{5}$$

$$\frac{\partial}{\partial t}(rJ\rho\varepsilon)+\frac{\partial}{\partial x^1}\left[rU_1\varepsilon-\frac{r}{J}(\mu+\frac{\mu_t}{\sigma_\varepsilon})\left\{\frac{\partial \varepsilon}{\partial x^1}B_1^1+\frac{\partial \varepsilon}{\partial x^2}B_2^1\right\}\right]$$
$$+\frac{\partial}{\partial x^2}\left[rU_2\varepsilon-\frac{r}{J}(\mu+\frac{\mu_t}{\sigma_\varepsilon})\left\{\frac{\partial \varepsilon}{\partial x^1}B_1^2+\frac{\partial \varepsilon}{\partial x^2}B_2^2\right\}\right]=rJ(C_{\varepsilon 1}\frac{\varepsilon}{k}G-C_{\varepsilon 2}\rho\frac{\varepsilon^2}{k}) \tag{6}$$

where

$$U_i=\rho u_k b_k^i,\ B_m^j=b_k^j b_k^m,\ w_j^i=\frac{\partial u_i}{\partial x^k}b_j^k \tag{7}$$

and

$$\mu_t=C_\mu\rho\frac{k^2}{\varepsilon} \tag{8}$$

$$G=\frac{\mu_t}{J^2}[2\left\{\frac{\partial u_1}{\partial x^1}b_1^1+\frac{\partial u_1}{\partial x^2}b_1^2\right\}^2$$
$$+2\left\{\frac{\partial u_2}{\partial x^1}b_2^1+\frac{\partial u_2}{\partial x^2}b_2^2\right\}^2\left\{\frac{\partial u_1}{\partial x^1}b_2^1+\frac{\partial u_1}{\partial x^2}b_2^2+\frac{\partial u_2}{\partial x^1}b_1^1+\frac{\partial u_2}{\partial x^2}b_1^2\right\}^2+2\frac{u_2^2}{r^2}] \tag{9}$$

$$C_{\varepsilon_1}=1.44,\ C_{\varepsilon_2}=1.92,\ P_\eta=0.9,\ C_\mu=0.09,\ \sigma_k=1.0,\ \sigma_\varepsilon=1.3 \tag{10}$$

In above equations U_i, T, k, ε denote two cylindrical velocity components, temperature, turbulent kinetic energy and rate of turbulent kinetic energy dissipation respectively. The geometric coefficients b_i^j represent the cofactors of $\partial y^j/\partial x^j$ in the Jacobian matrix of the coordinate transformation, J stands for the determinant of the Jacobian matrix, y^j is the cylindrical coordinate system and ρ,μ,p,P_r denote density, viscosity, pressure and Prandtl number respectively.

2.2.2 Discretization of Governing Equation

The solution domain is divided into a finite number of quadrilateral control volumes and the discretization of the governing equation is performed following the finite volume approach. The convection terms are approximated by a higer-order

bounded scheme HLPA developed by Zhu [3] and the unsteady terms are treated by the backward differencing scheme.

2.2.3. Momentum Interpolation Method

In the present study, the Rhie and Chows scheme [4] is modified to obtain a converged solution for unsteady flows which is independent of the size of time step and relaxation factors. The momentum equations are solved implicitly at the cell-centered locations in the Rhie and Chows scheme. The discretized form of momentum equations for the cell-centered velocity components can be written as follows with the under-relaxation factors expressed explicitly;

$$u_{1,P} = (H_{u_1})_P + (D^1_{u_1})_P (P_w - P_e)_P + (D^2_{u_1})_P (P_s - P_n)_P + (E_{u_1})_P u^{n-1}_{1,P} + (1-\alpha_{u_1}) u^{l-1}_{1,P} \tag{11}$$

$$u_{2,P} = (H_{u_2})_P + (D^1_{u_2})_P (P_w - P_e)_P + (D^2_{u_2})_P (P_s - P_n)_P + (E_{u_2})_P u^{n-1}_{2,P} + (1-\alpha_{u_2}) u^{l-1}_{2,P} \tag{12}$$

where

$$H_{u_i} = \alpha_{u_i} \left\{ \sum A^{u_i}_{nb} u_{i,nb} + (S^{u_i}_c \ \Delta V) \right\} \Big/ A^{u_i}_P \tag{13}$$

$$D^j_{u_i} = \alpha_{u_i} r\, b^j_i / A^{u_i}_P \tag{14}$$

$$E_{u_i} = \frac{\alpha_{u_i} \rho \Delta V}{\Delta t} \Big/ A^{u_i}_p \tag{15}$$

$$A^{u_i}_P = \sum A^{u_i}_{nb} - S^{u_i}_P \Delta V + \frac{\rho\, \Delta V}{\Delta t} \tag{16}$$

And α_{u_i} are the under-relaxation factors for u_i velocity components and the superscripts $n-1$, $l-1$ denote the previous time step and iteration level, respectively. The discretized form of momentum equations for the cell-face velocity component, for example u_1 at the east face, can be written as follows;

$$u_{1,e} = (H_{u_1})_e + (D^1_{u_1})_e (P_P - P_E) + (D^2_{u_1})_e (P_{se} - P_{ne}) + (E_{u_1})_e u^{n-1}_{1,e} + (1-\alpha_{u_1}) u^{l-1}_{1,e} \Big| \tag{17}$$

In the present modified Rhie and Chows scheme, this cell-face (the east face) velocity component is obtained explicitly through the interpolation of momentum equations for the neighboring cell-centered cylindrical velocity components. Following assumptions are introduced to evaluate this cell-face velocity component.

$$(H_{u_1})_e \approx f^+_e (H_{u_1})_E + (1 - f^+_e)(H_{u_1})_P \tag{18}$$

$$(D^2_{u_1})_e (P_{se} - P_{ne}) \approx f^+_e (D^2_{u_1})_E (P_s - P_n)_E + (1 - f^+_e)(D^2_{u_1})_P (P_s - P_n)_P \Big| \tag{19}$$

$$\frac{1}{(A^{u_1}_P)_e} \approx \frac{f^+_e}{(A^{u_1}_P)_E} + \frac{(1 - f^+_e)}{(A^{u_1}_P)_P} \tag{20}$$

where f_e^+ is the geometric interpolation factor defined in terms of distances between nodal points. Similar assumptions can be introduced for evaluating the velocity components at the north face. Using above assumptions, the velocity component $u_{1,e}$ can be obtained as follows;

$$u_{1,e} = \Big[f_e^+ u_{1,E} + (1-f_e^+)u_{1,P} + (D^1_{u_1})_e (P_P - P_E) - f_e^+ (D^1_{u_1})_E (P_w - P_e)_E - (1-f_e^+)(D^1_{u_1})_P (P_w - P_e)_P \Big] + (1-\alpha_{u_1})\Big[u^{l-1}_{1,e} - f_e^+ u^{l-1}_{1,E} - (1-f_e^+)u^{l-1}_{1,P} \Big] + \frac{\alpha_{u_1}\rho}{\Delta t}\left[\frac{(\Delta V)_e}{(A^{u_1}_P)_e} u^{n-1}_{1,e} - f_e^+ \frac{(\Delta V)_E}{(A^{u_1}_P)_E} u^{n-1}_{1,E} - (1-f_e^+)\frac{(\Delta V)_P}{(A^{u_1}_P)_P} u^{n-1}_{1,P} \right] \tag{21}$$

The term in the first bracket of right hand side of Eq. (21) is the original Rhie and Chows scheme [4]. Majumdar [5] has revealed that omission of the term in the second bracket leads to a converged solution which is relaxation factor dependent. Recently, Choi [6] added the term in the last bracket to obtain the converged solution that is independent of the size of time step and relaxation factors for unsteady flow calculations.

2.2.4. Solution Algorithm

The SIMPLEC algorithm by Van Doormal and Raithby [7] is used for pressure-velocity coupling in the present study. In this algorithm the momentum equations are implicitly solved at cell-centered locations using Eqs. (11) and (12). Then the cell-face velocities are evaluated by Eq. (21). Since these starred velocities do not satisfy the continuity equation unless the pressure field is correct, they should be corrected to satisfy the continuity equation during the iteration process. The following velocity correction equations are assumed in the SIMPLEC algorithm.

$$u'_{1,e} = u_{1,e} - u^*_{1,e} = (D^1_{u_1})_e (P'_P - P'_E) \Big/ \Big[1 - \alpha_{u_1} (\textstyle\sum A^{u_1}_{nb} / A^{u_1}_P)_e \Big] \tag{22}$$

$$u'_{2,e} = u_{2,e} - u^*_{2,e} = (D^1_{u_2})_e (P'_P - P'_E) \Big/ \Big[1 - \alpha_{u_2} (\textstyle\sum A^{u_2}_{nb} / A^{u_2}_P)_e \Big] \tag{23}$$

Inserting above equations into the continuity equation leads to a pressure correction equation. After solving the pressure correction equation, the cell-face velocities are corrected by above equations and the cell-centered velocities are corrected by following equations.

$$u'_{1,P} = u_{1,P} - u^*_{1,P} = \Big[(D^1_{u_1})_P (P'_w - P'_e) + (D^2_{u_1})_P (P'_s - P'_n) \Big] \Big/ \Big[1 - \alpha_{u_1} (\textstyle\sum A^{u_1}_{nb} / A^{u_1}_P)_P \Big] \tag{24}$$

$$u'_{2,P} = u_{2,P} - u^*_{2,P} = \Big[(D^1_{u_2})_P (P'_w - P'_e) + (D^2_{u_2})_P (P'_s - P'_n) \Big] \Big/ \Big[1 - \alpha_{u_2} (\textstyle\sum A^{u_2}_{nb} / A^{u_2}_P)_P \Big] \tag{25}$$

The pressure correction equations as well as other algebraic equations of momentum equations, energy equation and turbulent transport equations are solved by

the strongly implicit procedure by Stone [8] in the present study.

2.2.5. Treatment of Boundary Conditions

At the inlet both the velocity components and turbulent quantities are prescribed. At the outlet the zero gradient conditions are imposed while the velocity components are adjusted to satisfy the overall mass conservation. At the symmetry line the symmetry conditions are imposed. At the wall node both the velocity components are set to zero. For the near-wall control volumes, the wall shear-stress vector is expressed as a function of the nodal velocity component parallel to the wall. The wall shear stress is again decomposed in two components along u_1 and u_2, respectively, to be used as source terms in the corresponding momentum equations. The wall function method is used for the near-wall nodes.

3. Two Model Comparisons with Preliminary Analyses of the KALIMER

3.1 Constant Inlet Temperature Increase

The KALIMER design is a pool-type system, with the entirety of the primary heat transport system contained within the reactor vessel. During normal operation, the sodium core inlet and outlet temperatures are 386℃ and 530℃, and the other initial conditions used and important system parameters are listed in Table 1. In the case of two-dimensional model, the hot pool is modeled as shown in Fig. 3. The input parameters of the two-dimensional hot pool model named HP2D are core outlet temperature and flowrate. In the model, the temperature and velocity distributions in the hot pool are calculated.

Firstly, in the case of constant inlet temperature increase, we compare the prediction accuracy between one- and two-dimensional hot pool model. During normal operation, the sodium bulk temperature of the hot pool is 530℃ and flowrate is 2143.1kg/sec. Also the sodium velocity distribution in the hot pool is shown in Fig. 4. In the case that the hot pool sodium inlet temperature increases from 530℃ to 647℃ suddenly, the hot pool sodium temperature increases until it reaches to the inlet temperature. As shown in Fig. 5, the temperature behabiors of the both models are quite different. In the one-dimensional model, the outlet temperature increases slowly and immediately, and is reached to 645℃ after 420 seconds. However, in the two-dimensional model, the outlet temperature is not changed until 20 seconds and then increases steeply. The outlet temperature is reached to 645℃ after 250 seconds.

In two-dimensional model, the outlet sodium temperature is affected by the inlet sodium temperature change after several tens of seconds during normal operation and

is more actual qualitative prediction than one-dimensional model. The time delay can alter the overall reactor system response, so that it is necessary to predict the hot pool sodium temperature distribution with sufficient accuracy.

Table 1 Initial and key operating parameters

○ Power (MWth)	392.2
○ Number of IHTS loops	2
○ Cover gas pressure (MPa)	0.1013
○ Primary sodium flowrate (kg/s)	2143.1
○ Primary sodium core outlet temperature (℃)	530.0
○ Primary sodium core inlet temperature (℃)	386.2
○ Number of Primary pumps	4
○ Intermediate sodium flowrate (kg/s)	1803.6
○ IHX-IHTS inlet temperature (℃)	339.7
○ IHX-IHTS outlet temperature (℃)	511.0
○ Number of IHXs	4
○ Number of SGs	2
○ Steam flowrate (kg/s)	155.5
○ Steam temperature (℃)	483.2
○ Steam pressure (MPa)	15.5

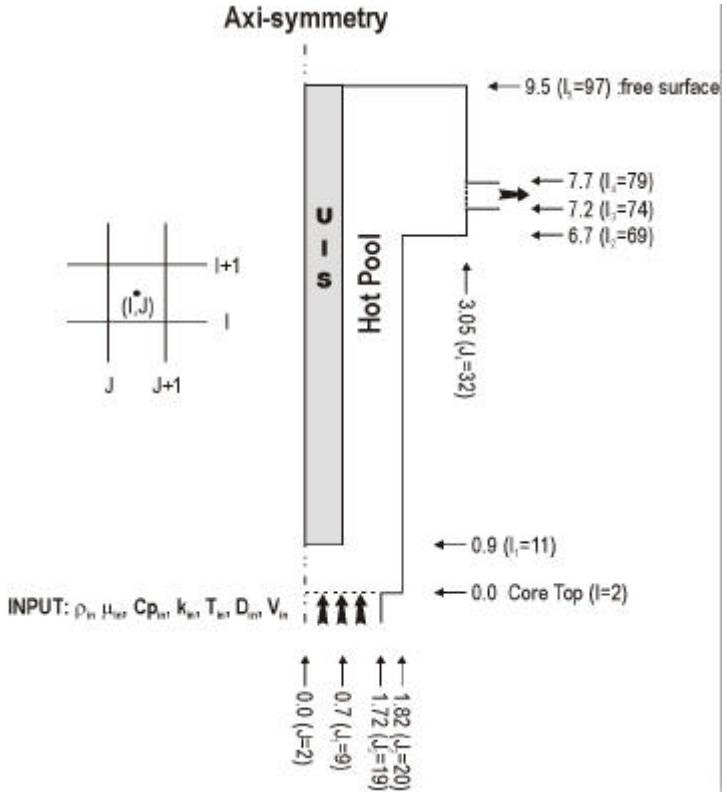

Fig. 3 Two-dimensional hot pool model

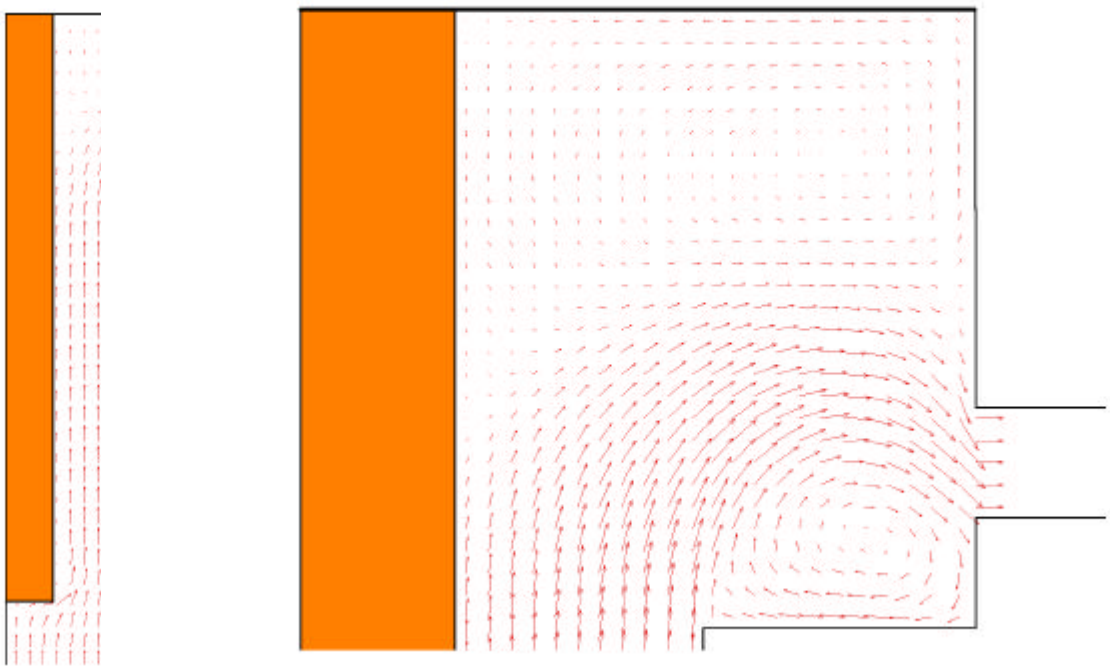

Fig. 4 Sodium velocity distribution in the hot pool during normal operation

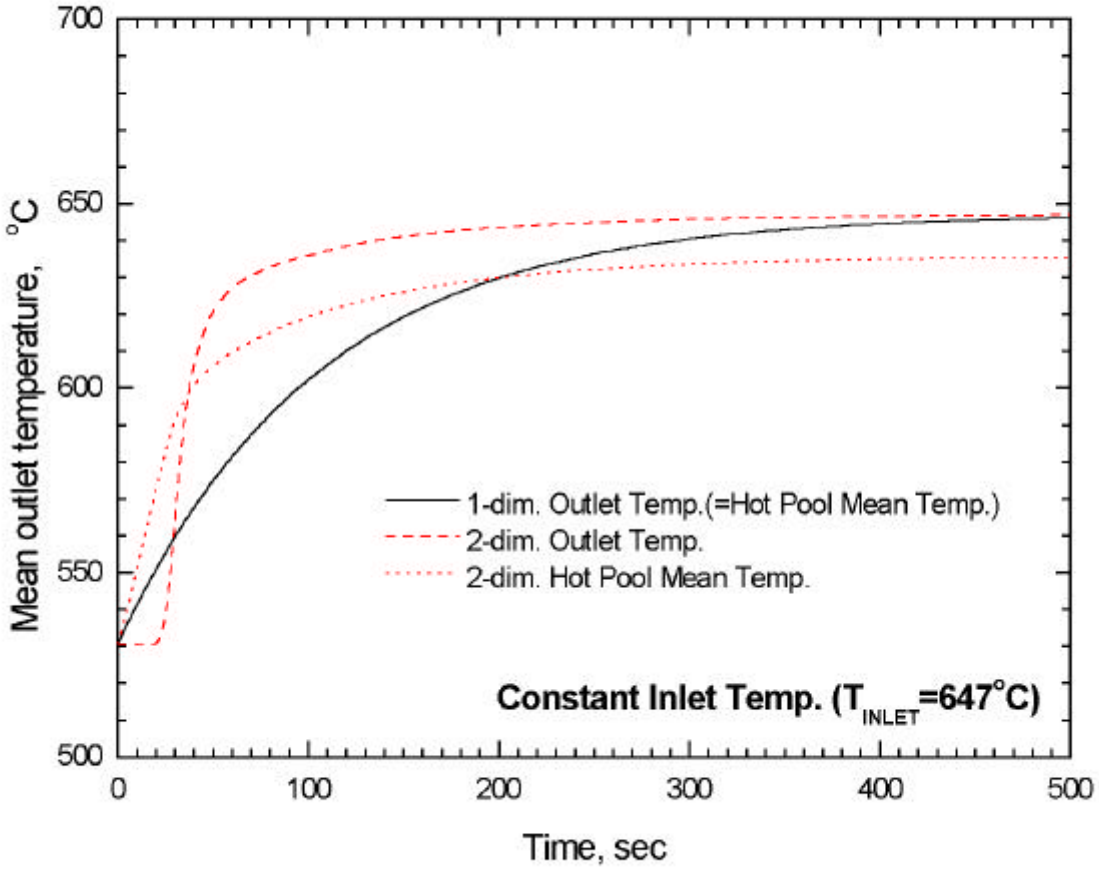

3.2 Unprotected Transient Overpower Events

An unprotected transient overpower (UTOP) event results when positive reactivity is inadvertently inserted into the core and there is a failure to scram. The limiting case assumption is that all the control rods are accidently removed. The event is initiated from full power. The control rods are assumed to begin withdrawing with a speed of 0.67 cents per second. The control rod stops are set to limit the withdrawal worth to 10 cents. The UTOP transient results for hot pool temperatures, power and flow in both cases of one- and two-dimensional models are shown in Fig. 6 through Fig. 8. As shown in Fig. 6, the power reaches a peak of 1.130 and 1.124 times the rated power at 34 and 27 seconds into the transient, and begins to level off at 1.019 and 1.021 times the rated power in the case of one- and two-dimensional model cases, respectively.

In the case of one-dimensional model, the hot pool inlet temperature increases from a normal value of 530℃ to a peak of 551℃ and outlet temperature increases from 530℃ to a peak of 543℃ and then the inlet and outlet temperatures are reestablished at around 542℃, which is 12℃ above the initial temperature, as shown in Fig. 7. On the other hand, in the case of two-dimensional model, the hot pool inlet temperature increases from 530℃ to 550℃ and outlet temperature increases from 530℃ to 546℃, and then the inlet and outlet temperatures are reestablished at around 543℃, which is 13℃ above the initial temperature. The outlet temperature is not affected by the inlet coolant until 25 seconds.

As a result of this comparison, it is considered that the time delay effect of the hot pool affects the core inlet sodium temperature. And then core inlet sodium temperature change affects the reactivity feedback and reactor power also. Therefore, it seems that the two-dimensional modeling of the hot pool can predict the overall reactor system response more realistic than one-dimensional model.

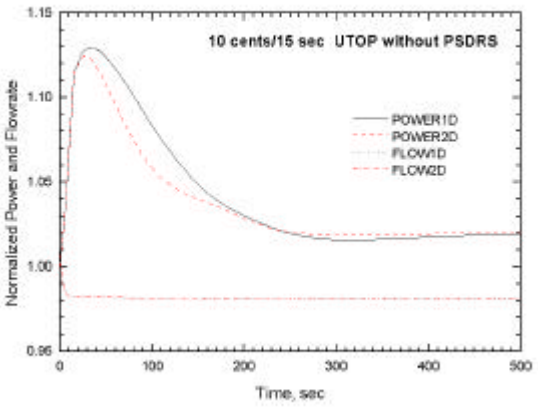

Fig. 6 Power and flow during 10 cent UTOP

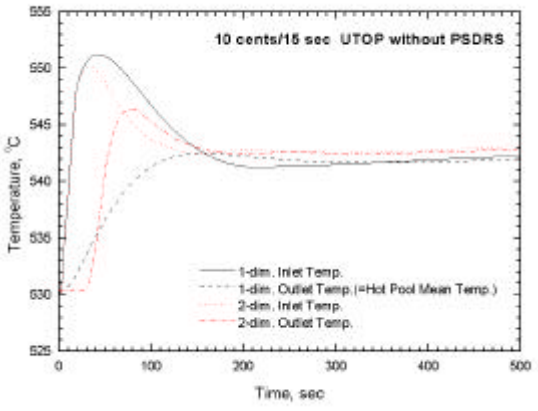

Fig. 7 Hot pool temp. during 10 cent UTOP

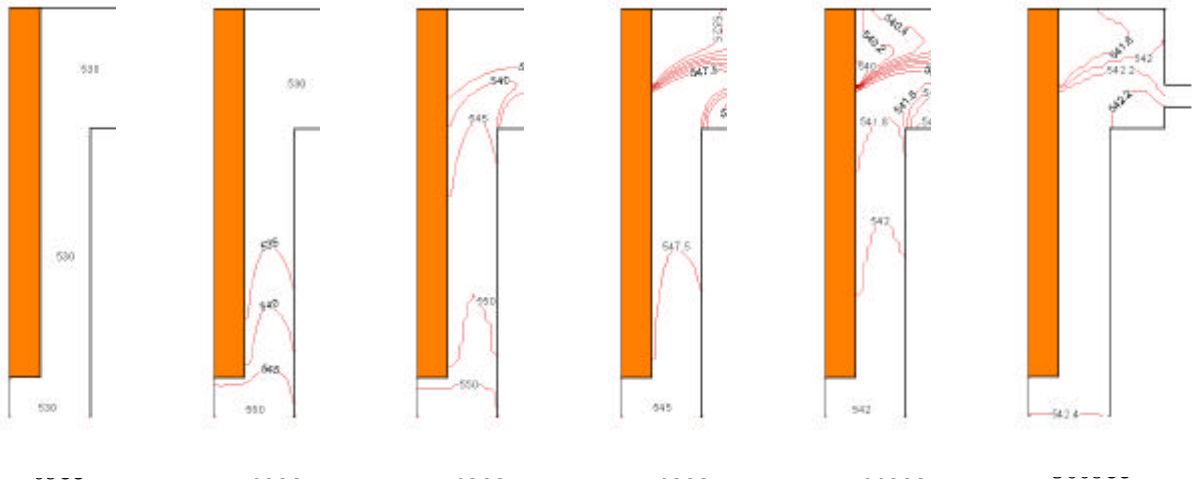

Fig. 8 Hot pool temperature distribution during 10 cent UTOP

4. Conclusions and Discussion

It is necessary to predict the hot pool sodium temperature distribution with sufficient accuracy to determine the core inlet temperature conditions. Therefore, two-dimensional hot pool model is developed and allpied to SSC-K pool-type LMR transient analysis computer code. From comparative results of predictions using the developed two-dimensional model and existing one-dimensional model some conclusions including recommendations for future works are as follows:

① In two-dimensional model, the time delay effect appears and is more actual qualitative prediction than one-dimensional model.

② The delayed time is a function of inlet flow conditions, i.e., flowrate and temperature difference between inlet and hot pool sodium temperature.

③ The time delay effect affects the reactivity feedback and power change. Therefore, it affects the overall reactor system response.

④ To validate the two-dimensional model qualitatively, it is necessary to compare the prediction results with the experimental data.

Acknowledgement

This work was performed under the long-term Nuclear R&D Program sponsored by the Ministry of Science and Technology.

References

[1] A.K. Agrawal et at., An Advanced Thermohydraulic Simulation Code for Transients in LMFBRs (SSC-L Code), BNL-NUREG-50773, Brookhaven Natinal Laboratory, 1973.

[2] C.K. Park et al., KALIMER Design Concept Report, KAERI/TR-888/97, 1997.

[3] J. Zhu, A Low-Diffusive and Oscillation Free Convection Schemes, Communications in Applied Numerical Methods, Vol. 7, pp. 225-232, 1991.

[4] C.M. Rhie and W. L. Chow, Numerical Study of the Turbulent Flow Past an Airfoil with Trailing Edge Separation, AIAA Journal, Vol. 21, pp. 1525-1532, 1983.

[5] S. Majumdar, Role of Under-relaxation in Momentum Interpolation for Calculation of Flow with Nonstaggered Grids, Numerical Heat Transfer, Vol. 13, pp. 125-132, 1988.

[6] S. K. Choi, Note on the Use of Momentum Interpolation Method for Unsteady Flows, Numerical Heat Transfer, Part A, Vol. 36, pp. 545-550, 1999.

[7] J. P. Van Doormal and G. D. Raithby, Enhancements of the SIMPLE Method for Predicting Incompressible Fluid Flows, Numerical Heat Transfer, Vol. 7, pp. 147-163, 1984.

[8] H. L. Stone, Iterative Solution of Implicit Approximations of Multi-dimensional Partial Differential Equations, SIAM Journal of Numerical Analysis, Vol. 5, pp. 530-558, 1968.